The TatA Subunit of *Escherichia coli* Twin-Arginine Translocase Has an N-in Topology†

Catherine S. Chan,‡ Marian R. Zlomislic,‡,§ D. Peter Tieleman,‡ and Raymond J. Turner*,‡

Department of Biological Sciences, and Department of Chemistry, University of Calgary, Calgary, Alberta T2N 1N4, Canada

Received March 15, 2007; Revised Manuscript Received April 17, 2007

ABSTRACT: The twin-arginine translocase (Tat) system is used by many bacteria to translocate folded proteins across the cytoplasmic membrane. The TatA subunit is the predicted pore-forming subunit and has been shown to form a homo-oligomeric complex. Through accessibility experiments using the thiol-reactive reagents 4-acetamido-4′-maleimidylstilbene-2,2′-disulfonic acid and N^{α}-(3-maleimidylproprionyl)-biocytin toward site-specific cysteine mutants in TatA, we show that the N-terminus of TatA is located in the cytoplasm rather than the previously assumed periplasm. We also confirm previous observations that the C-terminus has a dual topology. By treatment with the membrane uncoupler carbonyl cyanide-*m*-chlorophenyl hydrazone, we show that the topological state of the C-terminus is dependent on the membrane potential. These results suggest two architectures of TatA in the membrane: one with a single transmembrane helix and the other with two transmembrane helices. Molecular models of both topologies were used to develop and cartoon a homo-oligomeric complex as a channel with a diameter of ∼50 Å and suggest that the double transmembrane helix topology might be the building block for the translocation channel. Additionally, *in vivo* cross-linking experiments of Gly2Cys and Thr22Cys mutants showed that Gly2, at the beginning of transmembrane helix-1, is in close proximity with Gly2 of a neighboring TatA, as Cys2 cross-linked immediately upon the addition of copper phenanthroline. On the other hand, Cys22, at the other end of the transmembrane helix, took at least 10 min to cross-link, suggesting that a possible movement or reorientation is required to bring this residue into proximity with a neighboring TatA subunit.

The twin-arginine translocase (Tat)[1] system is used by many bacteria for translocating proteins across the cytoplasmic membrane (*1*, *2*). It is most distinctively different from the well-known Sec pathway in that it can translocate folded proteins, often with their cofactors inserted, and can even translocate heterodimeric complexes (*3*, *4*). Another unique feature of the Tat system is that its substrates possess a conserved SRRxFLK "twin-arginine" motif in their N-terminal signal sequences (*5*). The translocon is made up of the subunits TatA, TatB, and TatC. The current model identifies TatA as the pore-forming channel and TatBC as the substrate delivery vehicles to the TatA pore (*6*−*8*). The final component of the translocon is TatE, which is not required for translocation but has an interchangeable function with TatA (*2*).

Although TatA is the smallest subunit of the three proteins directly involved in translocation, it is hypothesized to form the transmembrane pore through homo-oligomerization, while translocation occurs via a relatively unknown mechanism. Early evidence of multimeric structures was demonstrated through low-resolution electron microscopy, showing a "double-layered ring" of reportedly six to seven TatA monomers forming a structure with a ∼65 Å central cavity (*9*). More recent studies were able to separate a range of TatA complexes ranging from 100 to 500 kDa in size, leading to a hypothesis that the pore adjusts to accommodate substrates of varying size (*10*). This hypothesis was further solidified when higher resolution imaging of the TatA complex demonstrated that it forms structures of a variety of sizes with similar architecture where it is a hollow ring with a "plug" at one end (*11*). The complexes varied in number of TatA subunits, from 12 to 35 monomers, and in channel diameter, from 30 to 70 Å. Furthermore, there is evidence in *Bacillus subtilis* that the homo-oligomeric TatA structure first forms in the cytoplasm, followed by insertion of the entire complex into the membrane through recruitment by TatC (*12*, *13*).

Information about the tertiary structure of TatA is limited. Secondary structure predictions and circular dichroism spectroscopy suggest that TatA consists of two α-helices at its N-terminus, one hydrophobic and one amphipathic, followed by a larger, unstructured C-terminus (*14*). Proteolytic assays show that the C-terminus of TatA exhibits dual topology because a tobacco etch virus (Tev) cleavage

† This work was supported by Canadian Institute of Health Research (CIHR) grants to R.J.T. and D.P.T. D.P.T. is an Alberta Heritage Foundation for Medical Research Senior Scholar and CIHR New Investigator.

* Corresponding author. Mailing address: Department of Biological Sciences, BI 156 Biological Sciences Bldg, University of Calgary, 2500 University Dr. NW, Calgary, Alberta, Canada T2N 1N4. Tel: 1-403-220-3581. Fax: 1-403-220-9311. E-mail: turnerr@ucalgary.ca.

‡ Department of Biological Sciences.

§ Department of Chemistry.

[1] Abbreviations: BM, biocytin maleimide, N^{α}-(3-maleimidylproprionyl)biocytin; CCCP, carbonyl cyanide-*m*-chlorophenyl hydrazone; CNS, crystallography and NMR system; CuP, copper(II) 1,10-phenanthroline; DMSO, dimethylsulfoxide; LB, Luria−Bertani; SDS, sodium dodecyl sulfate; SM, stilbene maleimide, 4-acetamido-4′-maleimidylstilbene-2,2′-disulfonic acid; Tev, tobacco etch virus; Tat, twin-arginine translocase; SCAM, substituted cysteine accessibility method.

10.1021/bi7005288 CCC: $37.00
Published on Web 05/31/2007

FIGURE 1: Point mutations of TatA used in this study. Single cysteine mutations were generated at the residues indicated, along with a C-terminal His_6 tag, then recombinantly expressed in *E. coli* JARV16, a strain lacking the TatA/E subunits. Predicted secondary structure elements helix-1 (a strongly predicted transmembrane segment) and helix-2 (an amphipathic helix) are illustrated.

site-fused TatA showed accessibility to Tev protease from both the cytoplasm and the periplasm (*15*). The N-terminus of TatA has been implied to be located in the periplasm based on predictions using the positive-inside rule and protease sensitivity experiments (*14*); however, this orientation has not yet been experimentally tested.

Proving the location of the N-terminus would limit the number of possible TatA topologies and improve understanding of its tertiary structure. As the purported pore-forming subunit of Tat, the architecture of TatA is likely to be a critical determinant of the translocation mechanism. Here we present experiments designed to target the location of the N-terminus. Using thiol-modifying reagents of opposite membrane permeability, we studied the ability of these reagents to access and modify cysteine residues mutated at strategic points in TatA (Figure 1) to determine the membrane location of these residues. Using this approach, the topology of the N-terminus of TatA was determined to be "N-in", where the N-terminus is exclusively located in the cytoplasm. Our studies also support that the C-terminus exhibits dual topology as described by other research (*15*). Here we also show that the topological state of the C-terminus is dependent on the membrane potential, whereas the N-terminal location remains unchanged under uncoupled conditions, limiting the dual topology model to only changes of the C-terminus. From these constraints on the termini and the predicted secondary structure, two possible configurations of TatA monomers in the bilayer can be inferred; one model has a single transmembrane helix (helix-1) and the other has two transmembrane helices (helix-1 and helix-2). The single transmembrane construct has a cytoplasmic N-terminus and periplasmic C-terminus whereas the double transmembrane construct has both N- and C-termini directed into the cytoplasm. These monomer topologies were used to construct 18-membered rings as models of the Tat translocation pore to critique their compatibility with findings about the three-dimensional structure of Tat complexes (*11*). *In vivo* cross-linking of residues surrounding helix-1 was also observed in this study, supporting other reports that TatA complexes are built from modular groupings of TatA subunits (*10*). Furthermore, rates of dimerization showed residue 2 of TatA to be in closer proximity with neighboring TatA, yet residue 22 is further away but may come into closer proximity after time or possibly as a result of movement, perhaps through a structural rearrangement due to the translocation function of TatA.

EXPERIMENTAL PROCEDURES

Construction of TatA Mutants. For a detailed list of primer sequences, please see Table 1. PCR amplification of *tatA* using pTatABC (*16*) as template by *Taq* DNA polymerase was performed with the primers TTAT5/TTAT2 to generate an *Eco*RI site upstream and a 6×His sequence and *Hin*dIII site downstream of *tatA*. The resulting PCR product and pBAD24 (*17*) were digested with *Eco*RI and *Hin*dIII, and the digested PCR product was ligated into pBAD24 at a insert/vector ratio of 3:1 using T4 DNA ligase at 4 °C overnight to generate the plasmid pTTAT1. G2C and V89C TatA:His_6 were generated in a similar fashion as above using the primers TTAT1/TTAT2 and TTAT5/TTAT19, respectively. The plasmids generated were pTTAT2 (G2C) and pTTAT9 (V89C). T22C, Insert (cysteine inserted between Thr22 and Lys23), and S44C TatA:His_6 were generated with the primers TTAT15/TTAT16, TTAT17/TTAT18, and TTAT9/TTAT10, respectively, using QuickChange II site-directed mutagenesis (Stratagene) to generate pTTAT10 (T22C), pTTAT11 (Insert), and pTTAT6 (S44C). All resulting plasmids were transformed into *Escherichia coli* JARV16 (*18*) via heat shock (*19*), and colonies selected for ampicillin resistance were then verified by sequencing through University Core Sequencing Services (University of Calgary, AB, Canada).

Growth Conditions. For functionality tests, starter cultures of *E. coli* MC4100, DADE (*20*), JARV16 (*18*), and JARV16 harboring the various TatA plasmids were grown in LB media containing 100 μg/mL ampicillin (for strains carrying plasmids) at 37 °C for 8 h and then diluted to the same OD_{600}. These were then used to subculture in 3 mL of LB media containing 2% (w/v) SDS and 0.02% (w/v) L-arabinose at a final concentration of 1% (v/v) and allowed to grow at 37 °C for 12 h at which time the OD_{600} was measured. Similarly, a 0.5% (v/v) subculture into glycerol DMSO minimal media (*21*) containing 0.01% (w/v) L-arabinose were grown anaerobically for 48 h. Cells were lysed by sonication and cytoplasmic and membrane fractions were isolated then tested for DMSO reductase activity as described in ref *21*.

For labeling and cross-linking studies, aerobic starter cultures were grown in LB media containing 100 μg/mL ampicillin at 30 °C for 16 h. Anaerobic cultures of 11.6 L containing 0.5% (v/v) starter culture in a peptone fumarate media (*22*) supplemented with 0.5% (v/v) glycerol and 100 μg/mL ampicillin were grown at 37 °C and induced with 0.02% (w/v) L-arabinose after 8 h. Cultures were allowed to grow for another 40 h then harvested by centrifugation at 1700 × *g*. Cells were washed with buffer A (5 mM NaH_2PO_4, 30 mM NaCl, pH 8.0) followed by resuspension in 2 times volume to wet pellet weight of buffer A. Uncoupled cells were generated by incubation of harvested, washed cells with 20 μM CCCP in buffer A at 37 °C for 1 h.

Cysteine Labeling. Cells were labeled immediately following harvest or uncoupling by incubating with 0.2 mM stilbene maleimide or biocytin maleimide (Molecular Probes, Invitrogen) for 30 min at room temperature on an end-over-end shaker. Stilbene maleimide-labeled cells were washed three times with buffer A then incubated with 0.2 mM biocytin maleimide as above. Both were then washed with buffer A containing 2% v/v β-mercaptoethanol, then again with buffer A.

Purification of TatA. Labeled cells from above were lysed through two passes through a French pressure cell at 16 000 psi, followed by centrifugation at 4000 × *g* to remove unlysed cells and debris, generating a clarified cell-free extract. Membrane vesicles were then isolated by ultracen-

Table 1: Primers Used in Generating the Various TatA Constructs[a]

primer	sequence (5′ to 3′)
TTAT1	TATAGAATTCAACATG**TGC**GGTATCAGTATTTG
TTAT2	TATAAAGCTTA*GTGATGGTGATGGTGATG*CACCTGCTCTTTATCGTG
TTAT5	TATAGAATTCACCATGGGTGGTATCAGTATTTG
TTAT9	GGCTTTAAAAAAGCAATG**TGC**GATGATGAACCAAAGCAGG
TTAT10	CCTGCTTTGGTTCATCATC**GCA**CATTGCTTTTTTAAAGCC
TTAT15	CGTTGTACTGCTTTTTGGC**TGC**AAAAAGCTCGGCTCCATCGG
TTAT16	CCGATGGAGCCGAGCTTTTT**GCA**GCCAAAAAGCAGTACAACG
TTAT17	GTACTGCTTTTTGGCACC**TGC**AAAAAGCTCGGCTCCATC
TTAT18	GATGGAGCCGAGCTTTTT**GCA**GGTGCCAAAAAGCAGTAC
TTAT19	ATATAAAGCTTA*GTGATGGTGATGGTGATG***GCA**CTGCTCTTTATCGTGGC

[a] The codon encoding the cysteine mutation is highlighted in bold, the codons encoding the His_6 tag are italicized, and restriction enzyme sites are underlined.

trifugation of the clarified cell-free extract at 100 000 × *g* for 1.5 h. Membrane vesicles were homogenized in buffer B (25 mM NaH_2PO_4, 150 mM NaCl, 5 mM imidazole, pH 8.0) and then solubilized with 2% (w/v) CHAPS (Anatrace) at 4 °C for 2 h while vortexing periodically. Insoluble material was removed by ultracentrifugation at 150000 × *g* for 40 min. TatA proteins were purified through nickel affinity on a HisTrap HP 1 mL column (Amersham Biosciences) using an ÄKTA purifier. Initially, a linear gradient up to 500 mM imidazole in buffer C [25 mM NaH_2PO_4, 150 mM NaCl, 0.37% (w/v) CHAPS, pH 8.0] was used to determine the optimal imidazole concentration to wash off contaminants. Final imidazole concentrations between 125 and 175 mM (depending on mutant) were used in a step gradient to wash off contaminants, followed by elution with 500 mM imidazole. Fractions containing TatA proteins as determined by tricine SDS−PAGE (see below) were pooled, then passed through a HiTrap desalting 5 mL column (Amersham Biosciences) to facilitate an exchange into buffer D (25 mM NaH_2PO_4, 150 mM NaCl, 0.37% w/v CHAPS, pH 7.4). Protein concentrations were determined by a modified Lowry method (*23*).

Detection of Biocytin Maleimide- or Stilbene Maleimide-Labeled Cysteines. Purified proteins were separated on a 12% tricine SDS−PAGE gel (*24*). Reducing agents were omitted from the sample incubation buffer due to the presence of dimeric forms through disulfide bonding. These dimers would contribute to a false negative signal because the reagents only label sulfhydryls in their reduced form. While a Lowry assay was used to determine the protein concentration, this was a combined concentration of monomers and dimers and would lead to biased results when detecting biocytin maleimide-labeled cysteines. Samples were electroblotted and probed against the His_6 tag using 1:1250 His-Probe HRP (Pierce) and detected via colorimetry using a HRP color development kit (Bio-Rad). Monomeric protein bands were quantitated based on their pixel densities using KODAK Gel Logic 100 software to determine the concentration of monomeric TatA in each sample. Samples containing 0.5 μg of monomer were then separated by tricine SDS−PAGE and electroblotted as above. The presence of biocytin maleimide-labeled cysteines was detected with 150 ng/mL streptavidin−HRP (Pierce) and developed as above.

The detection of stilbene maleimide-labeled cysteines was done through spectrophotometric absorbance of approximately 0.33 mg/mL purified protein at 322 nm. For better accuracy, protein concentrations were re-determined following absorbance measurements as described above. As a measurement of the degree of labeling, the moles of dye per mole of protein was determined by dividing the absorbance by the extinction coefficient of stilbene maleimide (35 000 M^{-1} cm^{-1}), then multiplying by the molar concentration of protein.

In Vivo Cross-Linking of TatA Mutants. Cells harvested as above were diluted another 15 times with buffer A and treated as described in ref *25*. Cells were incubated in 0.3 or 3 mM final concentration of CuP by mixing end-over-end; a 60 mM CuP stock contained 60 mM $CuSO_4$ and 200 mM 1,10-phenanthroline. Cells were incubated at room temperature for a total of 15 min where 1 mL was removed at 0, 2, 5, 10, and 15 min and added to a quench solution (final concentration of 8 mM *N*-ethylmaleimide and 10 mM EDTA). Prechilled cells were also incubated as above for 20 min at 4 °C and quenched for 10 min. Cells were collected by centrifugation and resuspended in 200 μL of sample incubation buffer lacking reducing agents then separated by tricine SDS−PAGE, electroblotted, and detected with His-Probe-HRP as above.

Modeling TatA Monomer Topologies and Multimeric Structures. The models presented here are based on a truncated version of TatA containing only residues 1−49. Residues 50−89 of TatA were not modeled because their secondary and tertiary structures are difficult to predict from the primary structure alone and because it has been shown that the Tat system can still function when truncated after 49 N-terminal residues (*26*). To model the single transmembrane construct of TatA, residues Gly21 to Lys23 were treated as an α−α-corner motif, and the remaining residues 1−49 were treated as an ideal helix. To accommodate the cytoplasmic N-terminus/cytoplasmic C-terminus topology, we treated amphipathic helix-2 as a transmembrane segment to generate a two-transmembrane-helix topology. A three-residue loop was modeled to generate this helical hairpin topology. The structures were energy minimized in a vacuum using the GROMOS96 43B1 (*27*) parameter set implemented in SwissPDB Viewer (*28*). Scaffolds for the 18-member TatA rings were generated using CNS (*29*) scripts with in-house modifications (*30*) to reproduce a circular distribution of single ideal helices in the *xy* plane with an interhelix distance restraint of 10.4 Å and a channel diameter of 50 Å. The protein topology parameters used were modified so that the side chain atoms had zero charge to prevent artificially strong interactions in the absence of explicit solvent (*31*). Images were rendered using Pymol (*32*).

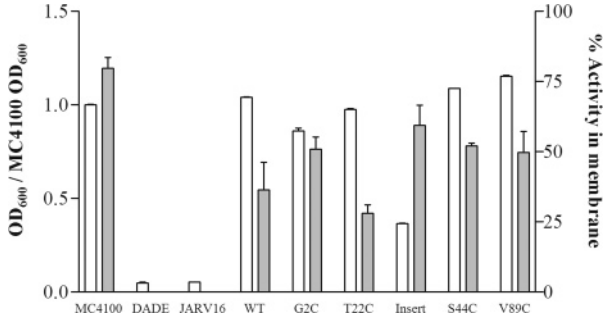

FIGURE 2: Functionality of TatA mutants. The normalized optical densities of cultures grown in the presence of 2% SDS (white bars) or percentage of DMSO reductase activity in the membrane fraction (gray bars) of *E. coli* MC4100, DADE (ΔtatABCD/E), JARV16 (ΔtatA/E), and JARV16 harboring plasmids expressing the various TatA mutants were determined. The DMSO reductase activities for DADE and JARV16 were not determined because these strains to not grow in glycerol DMSO minimal media.

RESULTS

Functionality of TatA Mutants. As shown in a previous study, media containing 2% (w/v) SDS was a simple and accurate test for the functionality of Tat subunits carrying single or truncating mutations (*33*). We used a similar test to ensure that our mutations (Figure 1) were not affecting the function and ability of TatA to translocate target proteins. In our initial experimental design, the previous observation that Thr22 was conserved for function (*26*, *34*, *35*) was taken into account; therefore, a T22C mutation and an insertional mutation where the cysteine was inserted between Thr22 and Lys23 were both generated to determine which of the two was more suitable in terms of viability for our topology experiments. We found that except for Insert TatA, the expression of the various mutants in *E. coli* JARV16, a strain that is devoid of its TatA/E subunits, was able to restore the growth to near that of the MC4100 wild-type strain (Figure 2, white bars). Our results show that while Thr22 was previously shown to be important for function, the insertion of cysteine after this residue was more detrimental than mutating it; therefore all of the following experiments were performed on the T22C mutant instead. This assay also showed that the restoration of Tat functionality was solely due to our mutants because cultures without arabinose to induce the expression of the constructs resulted in no growth in the presence of SDS (results not shown). Since DMSO reductase has been shown to be Tat-dependent for targeting to the cytoplasmic membrane and is involved in anaerobic respiration in *E. coli* (*22*), the percentage of DMSO reductase activity in the membrane fractions isolated from cells grown in glycerol DMSO minimal media were also investigated (Figure 2, gray bars). The results from this assay showed a lesser degree of restoration by the expression of the plasmids due to the low concentration of inducer used to express the constructs. However, since DADE and JARV16 were unable to even grow in the minimal media used in this assay, the activity results further support that TatA is still functioning properly even with the various mutations.

Topology of TatA through Accessibility of Thiol-Modifying Reagents. The use of substituted cysteine accessibility method (SCAM; reviewed in ref *36*) is a popular and established technique to study membrane boundaries and topologies of many integral membrane proteins containing

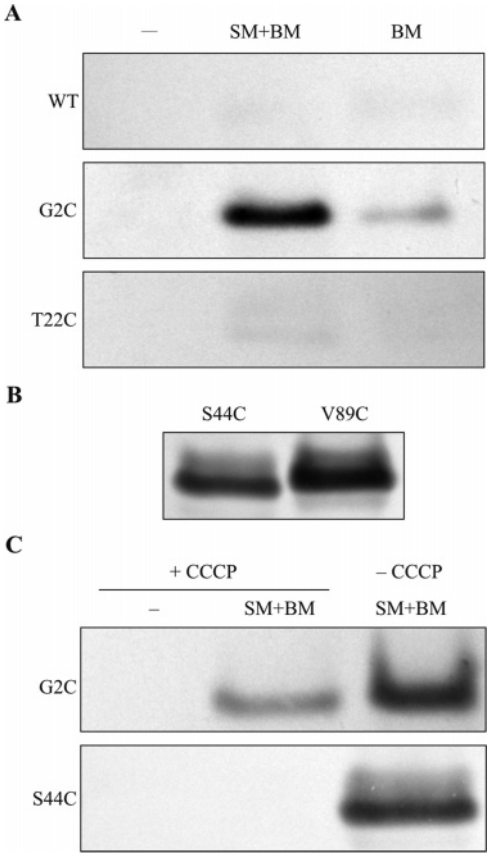

FIGURE 3: The topology of TatA—Western blot analysis of TatA mutants. Equal amounts of monomeric protein were detected for biocytin maleimide-labeled cysteines through binding of streptavidin. In panel A, WT, G2C, and T22C TatA were either unlabeled (−), labeled with stilbene maleimide and then biocytin maleimide (SM+BM), or labeled only with biocytin maleimide (BM). In panel B, S44C and V89C TatA mutants were labeled with stilbene maleimide then biocytin maleimide. In panel C, G2C and S44C TatA were untreated (− CCCP) or pretreated (+ CCCP) with the membrane uncoupler CCCP and then left unlabeled (−) or labeled with stilbene maleimide and then biocytin maleimide (SM+BM).

single or multiple transmembrane helices (*25*, *37*−*51*). SCAM is based on the use of covalent thiol-modifying reagents against the target protein, which is mutated to contain single cysteine residues at the boundaries of the transmembrane helices or along the entire protein in more extensive studies. In combination with thiol-modifying reagents of opposing membrane permeability, the topological orientation of such proteins can be determined. In our study, residues corresponding to regions that surround each predicted secondary structure zone in TatA were mutated to cysteine (Figure 1), and then labeled by the impermeant reagent stilbene maleimide and the permeant reagent biocytin maleimide. Purified TatA proteins isolated from whole cells that were unlabeled (−), labeled with stilbene maleimide and then biocytin maleimide (SM+BM), or labeled with only biocytin maleimide (BM) were detected via a Western blot probed with streptavidin, which only binds the biotin derivative on biocytin maleimide (Figure 3A). When one looks at the results from G2C and T22C TatA, it is apparent that G2C was labeled by biocytin maleimide and T22C was not (Figure 3A, SM+BM lanes). The faint signal observed in the WT lanes was due to a slight excess of streptavidin resulting in nonspecific binding as blots incubated with less streptavidin did not show any signal, making the faint signal

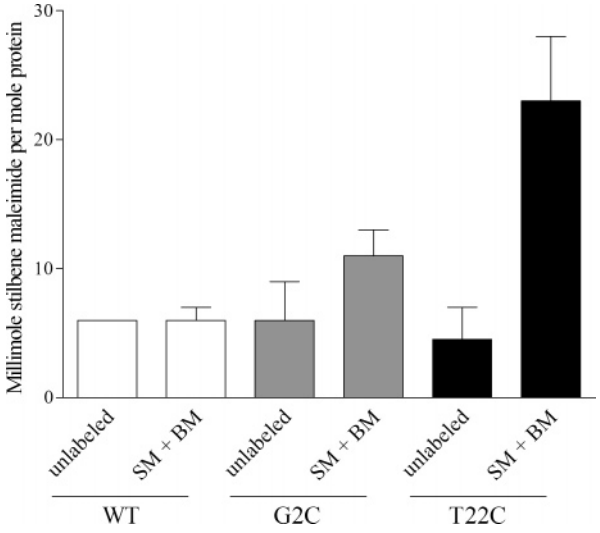

FIGURE 4: Labeling of TatA proteins by stilbene maleimide. The presence of stilbene maleimide-labeled cysteine residues were determined by measuring the absorbance of stilbene maleimide at 322 nm. The moles of stilbene maleimide per mole of protein for three measurements of each was calculated and plotted.

in the T22C lanes negligible. This also shows that the signal observed in the G2C SM+BM lane (Figure 3A) was due to the binding of biocytin maleimide to the cysteine residue and not other regions of the protein. Because G2C TatA was labeled by biocytin maleimide, this indicates that the cysteine is located in the cytoplasm due to the order in which the cells were labeled. Since the whole cells were incubated with the impermeant stilbene maleimide first, only periplasmic cysteines would be labeled by it. Incubation with the permeant biocytin maleimide afterward results in labeling of only cytoplasmic cysteines by biocytin maleimide because stilbene maleimide labeling of periplasmic cysteines is irreversible. Based on this analogy, the cysteine in G2C TatA must be located in the cytoplasm in order to be labeled by biocytin maleimide. The absence of detection by streptavidin toward T22C TatA showed that the cysteine in this mutant was not labeled by biocytin maleimide (Figure 3A, SM+BM lane), implying that it was labeled by stilbene maleimide, and therefore it is located in the periplasm. Labeling of TatA by stilbene maleimide was confirmed through measuring its absorbance at 322 nm, where the moles of dye per mole of protein was much higher for T22C TatA than G2C TatA (Figure 4), providing yet further evidence for labeling interpretations.

Labeling of G2C TatA by biocytin maleimide appeared to be weaker in the absence of stilbene maleimide (Figure 3A, G2C BM lane), which is likely due to the limiting concentrations of reagents used. In this situation, cysteines of periplasmic proteins and periplasmically located regions of integral membrane proteins are also competing for this reagent. In contrast, cells pretreated with stilbene maleimide will have their periplasmic cysteines modified; thus they are unable to compete for biocytin maleimide. This competition effect is further exacerbated when biocytin maleimide must also cross the cytoplasmic membrane prior to reaching cytoplasmically located cysteines, leading to the observed results for both mutants (Figure 3A, BM lanes). Furthermore, labeling of T22C TatA by stilbene maleimide was verified through its absorbance as mentioned above, indicating that even though accessibility of biocytin maleimide appears

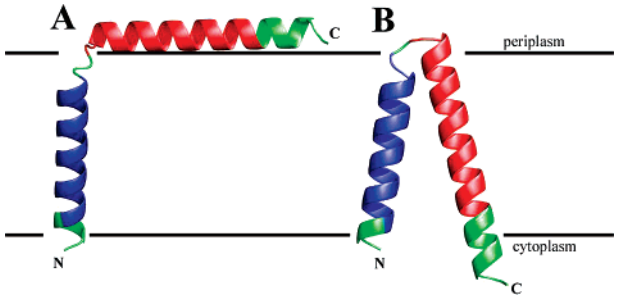

FIGURE 5: Two models of TatA monomers using residues 1−49. Predicted helix-1 residues (4−20) are colored blue; predicted helix-2 residues (23−41) are colored red. The remaining residues in $TatA^{1-49}$ are colored green: (A) single transmembrane orientation; (B) double transmembrane orientation.

weaker toward this cysteine, this potential competition or inaccessibility effect has little implication on the derived topological results. Further experiments using 3-fold increase of reagent and doubled labeling times did not significantly alter biocytin maleimide labeling but showed an increase of labeling by stilbene maleimide (results not shown), further supporting the above topology results.

Labeling experiments were also performed on whole cells isolated from cultures expressing S44C or V89C TatA mutants and results show that the cysteines in these two mutants were labeled by biocytin maleimide (Figure 3B). This suggests that the C-terminal region of TatA following helix-2 is located in the cytoplasm. In combination with the N-terminal data, TatA has a two transmembrane structure with both N- and C-termini located in the cytoplasm. Taking into account that other researchers showed dual topology of the TatA C-terminus (*15*), it was recognized that our labeling method would not be able to detect the population of TatA whose C-termini are located in the periplasm unless performed on everted vesicles. However, since we were unable to generate a population containing 100% everted vesicles with certainty by passing through a French pressure cell, a different method was employed. Given the prior observation that translocation of SufI by Tat can be blocked by the addition of the membrane uncoupler CCCP (*16*) and that the dual topology is suggested to have a role in the translocation cycle (*15*), we sought to test this hypothesis by the addition of CCCP to cells expressing the S44C mutant prior to labeling. The results from this experiment show that S44C TatA isolated from CCCP-treated cells was not labeled by biocytin maleimide (Figure 3C), indicating that this residue is now located in the periplasm. In order to test that the addition of CCCP had no effect on the accessibility of the thiol-modifying reagents toward cysteine residues, the same experiment performed on cells expressing G2C TatA showed that while labeling was slightly weaker when pretreated with CCCP, this was not sufficient to completely block cysteine-labeling by biocytin maleimide (Figure 3C).

These results lead to an upside-down L-shaped topology with the N-terminus in the cytoplasm and C-terminus in the periplasm when the membrane potential is uncoupled. The G2C results also show that the N-terminal end of TatA is always anchored to the cytoplasm and previous observations of dual topology are due to mixed topologies of the C-terminus only. In combination with the topology results with an intact membrane potential, two different models of TatA are generated (Figure 5).

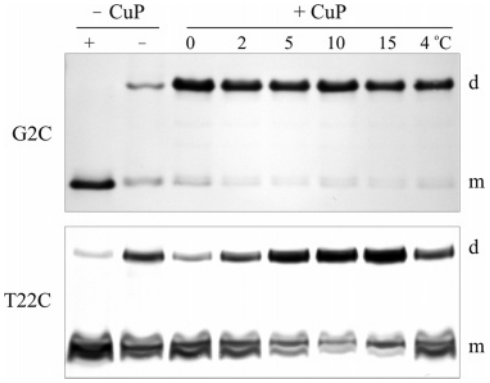

FIGURE 6: *In vivo* cross-linking of G2C and T22C TatA. Western blot analysis of TatA through detection against the His_6 tag. Samples that were not incubated with any cross-linker (− CuP) were separated via tricine PAGE in the presence (+) and absence (−) of 2% β-mercaptoethanol. Samples incubated with cross-linker (+ CuP) at room temperature, periodically quenched at fixed time intervals (expressed in minutes) or prechilled and incubated for 20 min (4 °C), were separated without any reducing agents. The monomeric (m) and dimeric (d) forms were determined based on the apparent molecular weights compared with protein standards.

Cross-Linking Studies of G2C and T22C TatA. All four of the TatA mutants appeared to form dimers based on PAGE and Western analysis (results not shown). However, the dimers could be resolved into the monomer form through the addition of β-mercaptoethanol to the samples (results not shown), indicating that these dimers were due to the formation of disulfide bonds. In order to demonstrate that the dimeric forms were not a result of the downstream processing procedures, *in vivo* cross-linking experiments were performed. The addition of CuP would permanently trap cysteines within close proximity in a cross-linked form, and the rate of cross-linking would also reflect the degree of closeness of these cysteines. This technique has been successfully utilized in mapping the spatial proximities of transmembrane helix movements in the bacterial chemoreceptor Trg during signaling (*52*, *53*). For both mutants, a small portion of the protein was present as a dimer prior to cross-linking because samples not incubated with CuP showed small amounts in the dimer form (Figure 6, − CuP lanes). Furthermore, a small population of the protein remained in the monomer form regardless of the length of incubation with CuP (Figure 6, + CuP lanes). Incubation of G2C TatA cells with both 0.3 (results not shown) and 3 mM CuP showed that it dimerized immediately upon the addition of CuP, whereas T22C TatA did not reach a saturation of dimers until at least 10 min (Figure 6). Since the rate of cross-linking is dependent on the proximity of cysteine residues, these results suggest that Cys2 residues are in closer proximity than Cys22 residues. When cells were prechilled prior to cross-linking, the amount of dimer formed was the same for G2C TatA but was lower for T22C TatA even though they were incubated for a total of 20 min (Figure 6, lanes 4 C). At this temperature, the rotational and translational diffusion of TatA subunits would be slower, contributing to the slower rate of dimerization in T22C TatA. This observation again suggests that Cys2 residues are in close proximity and Cys22 residues become close to each other over time.

Modeling TatA Monomer Topologies and Multimeric Structures. Based on the topology results above, two possible topologies of monomeric TatA that illustrate these results are shown in Figure 5. The predicted secondary structure of TatA was considered with the two topologies observed: cytoplasmic N-terminus/periplasmic C-terminus and cytoplasmic N-terminus/cytoplasmic C-terminus. Helix-1 of TatA is strongly predicted to be transmembrane and is linked to the proposed amphipathic helix-2 by a very short linker region of two to three residues. We also explored modeling of a multimeric TatA ring using both topologies obtained above for global comparisons to the electron microscopy structures observed in ref *11*. Viewed from the *z*-axis, our models show a channel with diameter of 45−50 Å (Figure 7), consistent with class 4 TatA complexes observed by electron microscopy (*11*). The structures of ideal single helices served as scaffolding upon which complete TatA (residues 1−49) topologies could be modeled. In the case of the single transmembrane topology, helix-1 would be the pore-lining helix (modeled by Ile6−Leu18 in CNS). In the case of the double transmembrane topology, helix-2 would be the pore-lining helix (modeled by Leu25−Phe39 in CNS). The 18-mer scaffolds were imported to SwissPDB Viewer, where the ideal monomer topologies were fit onto the scaffolds to generate complete $TatA^{1-49}$ 18-mer structures as possible models of the Tat translocating pore (Figure 7).

DISCUSSION

The Tat system has been identified as a secondary protein translocation pathway in bacteria and yet its mechanism of function is still largely unknown. While it is accepted that there are three subunits that make up the translocon, TatA is generally thought to serve as the channel that allows proteins to cross the cytoplasmic membrane and is an essential component of the translocase. The complete topology of TatA is a key element for understanding the architecture and thus its translocation mechanism at a molecular level. While the topology of TatA has been studied using reporter fusions and proteolytic assays toward its C-terminus, the sided-ness and orientation of the N-terminus

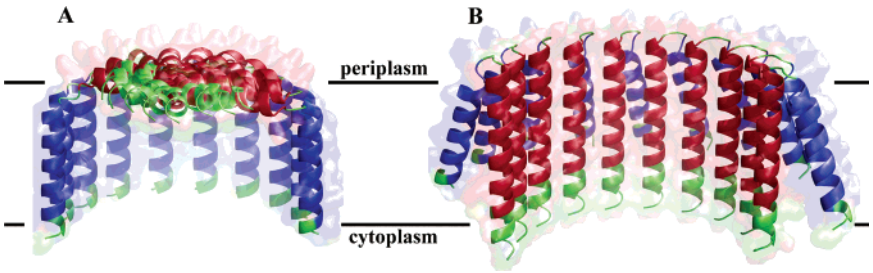

FIGURE 7: Models of the 18-mer $TatA^{1-49}$ complexes. The structures are shown as a cut-through representation to illustrate the interior and exterior of the proposed channel: (A) single transmembrane structure; (B) double transmembrane structure. Both channels have diameter ~50 Å, but the wall diameter of B is ~25 Å. Helix-2 (red) in model A has extreme steric clashes between neighboring and opposite helices.

has only been implied based on the results of the C-terminus. Here we determined the orientation of both the N- and C-terminus. Using four TatA cysteine point mutants surrounding key structural regions (Figure 1), we were able to establish a topological orientation of TatA where it is upside down and opposite to that shown in recent reviews and models (*15*, *54*). Its N-terminus is in the cytoplasm, while the rest of the protein exhibits two different topological orientations depending on the presence of an intact membrane potential (Figure 5).

The choice of using covalent sulfhydryl modifying reagents targeted to single cysteine mutants in TatA, rather than using reporter fusions, to study its N-terminal location is due to the artificially induced topological orientation that the reporter fusions could generate. Furthermore, a single mutation to a cysteine residue is less likely to perturb the function of TatA in comparison to the addition of a reporter fusion, regardless of how small this fusion may be. Topological determination using a single cysteine-directed labeling approach has been successfully used to study many membrane proteins. Examples include determining the membrane topology of the α-subunit of the *E. coli* F_1F_0 ATP synthase (*49*) and demonstrating topological dependence of LacY from *E. coli* lactose permease on phospholipid composition (*50*).

Our results support that the C-terminus of TatA has dual topology (Figure 5); however, it was only observed as the single topology with the C-terminus in the periplasm when the membrane potential was removed by the membrane uncoupler CCCP. This reagent was successfully utilized in previous studies to block *in vivo* and *in vitro* translocation of SufI by the Tat translocon (*16*). Based on our results, it is apparent that the two topological states are dependent on the ΔpH across the cytoplasmic membrane, and it is possible that these two topological states of TatA represent the inactive and active translocating state of TatA in the translocation cycle. The single transmembrane topology determined from our uncoupled membranes is likely the orientation of inactive TatA.

The dual topology of the TatA C-terminus was first suggested by studies done by Gouffi et al. (*15*) and is now supported here by a different approach. However, in studies by Gouffi et al., the N-terminus of TatA was implied to be located in the periplasm, a conclusion that was also implied by Porcelli et al. (*14*) who performed protease sensitivity experiments and found the C-terminal region of TatA to be accessible from the periplasm. While results from both groups agree with each other (and results shown here) in terms of the C-terminus, they presented no experimental data that support the location of the N-terminus. Most sequence analysis algorithms predict that the N-terminus is located in the periplasm, although TMbase (*55*) predicts that the N-terminus is located in the cytoplasm. TatA theoretically would have its N-terminus located in the periplasm based on the positive-inside rule (*56*) due to residues Lys23 and Lys24 following helix-1. However, given the possibility that helix-2 may form a transmembrane helix as indicated by its dual topology, residues Lys40 and Lys41 (and possibly Lys37, which may or may not be part of helix-2 depending on the secondary structure prediction algorithm used), would fall on the cytoplasmic side of the membrane, leading to the positive-inside rule being obeyed and supporting our model. Given that examples of flip-flopping, topologically confused membrane proteins (whereby a membrane protein without a significant charge bias to determine its topology is inserted in multiple orientations) have been recently suggested (*57*), it is possible that TatA may also fall into this category of proteins.

The dimeric forms observed with the G2C and T22C mutants also give insight in the interactions of helix-1 with helices of neighboring TatA molecules during oligomerization. *In vivo* cross-linking experiments show that the residues 2 (glycine) of neighboring helices in the oligomeric form may be in closer proximity than residues 22 (threonine). This trend was observed even during lower temperatures where the movement of TatA helices would be slower, indicating that residue 2 in TatA is likely always in close proximity to its neighbor, whereas residue 22 must exhibit some flexibility in movement, leading to the slower rate of cross-linking. The slower cross-linking of residue 22 may reflect movement of TatA helices during translocation. The observation that these mutants cross-link also supports the homo-oligomeric model of the TatA pore described in other publications (*9*, *11*). The slower cross-linking rate of residue 22 may be a result of reduced accessibility of the cross-linker to this residue. However, the possibility of movements in TatA still exist, since this method was successfully used in spatial mapping of transmembrane helix movements of the Trg chemoreceptor during signaling (*52*, *53*).

The two distinct topologies have significant implications for the structure of the translocating pore. Secondary structure prediction from the sequence of TatA in conjunction with the N-in topology presented here suggest an L-shaped structure of the monomer (Figure 5A). If we assume that the monomeric structure does not change when TatA assembles into a multimeric structure, and we generate an 18-membered ring with a diameter of ∼50 Å (Figure 7A is a cut through of this structure), we can clearly see that what we have denoted as helix-2 (Figure 1) cannot reside as an interfacial helix in this context. An interfacial helix of ∼20 residues cannot sit in this geometrical structure without severe steric clashes. This suggests that if the translocating pore is constructed of single transmembrane TatA monomers, the "capping" residues must have some other structural motifs than interfacial helices. Another problem with the single transmembrane homo-oligomeric complex is that the hydrophobic character of the pore-lining helices would require that it be solvated with lipids, not water or air. In this case, it is difficult to imagine the energetic cost of reorganizing the lipids in a cavity with a 50 Å diameter. Based on these observations, the single transmembrane topology as depicted in Figure 5A may be structurally stable as a monomer, but it must undergo some structural rearrangement to function in a multimeric translocating pore.

In contrast, the double transmembrane topology illustrated in Figure 5B cannot sit as a monomer in the membrane because of the number of polar and charged residues in helix-2. However, this topology could assemble readily into a multimeric structure (Figure 7B). The charged and polar residues of helix-2 might line the pore interior and then be solvated by water, while the hydrophobic outer-ring formed by helix-1 is solvated by the membrane. The dimensions of this construct are in agreement with the structure analysis of class 4 TatA complexes in ref *11*. The model presented here is primarily based on meeting the constraints imposed

on the topology of TatA set by the results of the accessibility experiments presented here, in connection with secondary structure predictions. Detailed residue interactions are not provided by these models but warrant further study. To date, there are no proteins of known structure with homologous sequences to TatA. More detailed structural information such as the secondary structure of helix-2 and characterizations of residues 50−89 will be essential to a complete description of the TatA oligomeric complex and how it functions as a translocating pore.

The topology and modeling results presented here provide a new view of the TatA topology, give further insight toward the function of TatA, and have implications toward the translocation mechanism.

ACKNOWLEDGMENT

We thank Frank Sargent (University of East Anglia Norwich, Norfolk, U.K.) for the generous donation of the *E. coli* JARV16 and DADE strains. We also thank Tara Winstone and Walter Ash (University of Calgary, Calgary, AB, Canada) for technical assistance and for use of his modified CNS scripts, respectively.

REFERENCES

1. Weiner, J. H., Bilous, P. T., Shaw, G. M., Lubitz, S. P., Frost, L., Thomas, G. H., Cole, J. A., and Turner, R. J. (1998) A novel and ubiquitous system for membrane targeting and secretion of cofactor-containing proteins, *Cell 93*, 93−101.
2. Sargent, F., Bogsch, E. G., Stanley, N. R., Wexler, M., Robinson, C., Berks, B. C., and Palmer, T. (1998) Overlapping functions of components of a bacterial Sec-independent protein export pathway, *EMBO J. 17*, 3640−3650.
3. Rodrigue, A., Chanal, A., Beck, K., Muller, M., and Wu, L. F. (1999) Co-translocation of a periplasmic enzyme complex by a hitchhiker mechanism through the bacterial Tat pathway, *J. Biol. Chem. 274*, 13223−13228.
4. Wu, L. F., Chanal, A., and Rodrigue, A. (2000) Membrane targeting and translocation of bacterial hydrogenases, *Arch. Microbiol. 173*, 319−324.
5. Berks, B. C. (1996) A common export pathway for proteins binding complex redox cofactors? *Mol. Microbiol. 22*, 393−404.
6. Palmer, T., Sargent, F., and Berks, B. C. (2005) Export of complex cofactor-containing proteins by the bacterial Tat pathway, *Trends Microbiol. 13*, 175−180.
7. Berks, B. C., Palmer, T., and Sargent, F. (2005) Protein targeting by the bacterial twin-arginine translocation (Tat) pathway, *Curr. Opin. Microbiol. 8*, 174−181.
8. Sargent, F., Berks, B. C., and Palmer, T. (2006) Pathfinders and trailblazers: a prokaryotic targeting system for transport of folded proteins, *FEMS Microbiol. Lett. 254*, 198−207.
9. Sargent, F., Gohlke, U., De Leeuw, E., Stanley, N. R., Palmer, T., Saibil, H. R., and Berks, B. C. (2001) Purified components of the *Escherichia coli* Tat protein transport system form a double-layered ring structure, *Eur. J. Biochem. 268*, 3361−3367.
10. Oates, J., Barrett, C. M., Barnett, J. P., Byrne, K. G., Bolhuis, A., and Robinson, C. (2005) The *Escherichia coli* twin-arginine translocation apparatus incorporates a distinct form of TatABC complex, spectrum of modular TatA complexes and minor TatAB complex, *J. Mol. Biol. 346*, 295−305.
11. Gohlke, U., Pullan, L., McDevitt, C. A., Porcelli, I., de Leeuw, E., Palmer, T., Saibil, H. R., and Berks, B. C. (2005) The TatA component of the twin-arginine protein transport system forms channel complexes of variable diameter, *Proc. Natl. Acad. Sci. U.S.A. 102*, 10482−10486.
12. Schreiber, S., Stengel, R., Westermann, M., Volkmer-Engert, R., Pop, O. I., and Muller, J. P. (2006) Affinity of TatCd for TatAd elucidates its receptor function in the *Bacillus subtilis* twin arginine translocation (Tat) translocase system, *J. Biol. Chem. 281*, 19977−19984.
13. Westermann, M., Pop, O. I., Gerlach, R., Appel, T. R., Schlormann, W., Schreiber, S., and Muller, J. P. (2006) The TatAd component of the *Bacillus subtilis* twin-arginine protein transport system forms homo-multimeric complexes in its cytosolic and membrane embedded localisation, *Biochim. Biophys. Acta 1758*, 443−451.
14. Porcelli, I., de Leeuw, E., Wallis, R., van den Brink-van der Laan, E., de Kruijff, B., Wallace, B. A., Palmer, T., and Berks, B. C. (2002) Characterization and membrane assembly of the TatA component of the *Escherichia coli* twin-arginine protein transport system, *Biochemistry 41*, 13690−13697.
15. Gouffi, K., Gerard, F., Santini, C. L., and Wu, L. F. (2004) Dual topology of the *Escherichia coli* TatA protein, *J. Biol. Chem. 279*, 11608−11615.
16. Yahr, T. L., and Wickner, W. T. (2001) Functional reconstitution of bacterial Tat translocation in vitro, *EMBO J. 20*, 2472−2479.
17. Guzman, L. M., Belin, D., Carson, M. J., and Beckwith, J. (1995) Tight regulation, modulation, and high-level expression by vectors containing the arabinose PBAD promoter, *J. Bacteriol. 177*, 4121−4130.
18. Sargent, F., Stanley, N. R., Berks, B. C., and Palmer, T. (1999) Sec-independent protein translocation in *Escherichia coli*. A distinct and pivotal role for the TatB protein, *J. Biol. Chem. 274*, 36073−36082.
19. Hanahan, D. (1983) Studies on transformation of *Escherichia coli* with plasmids, *J. Mol. Biol. 166*, 557−580.
20. Wexler, M., Sargent, F., Jack, R. L., Stanley, N. R., Bogsch, E. G., Robinson, C., Berks, B. C., and Palmer, T. (2000) TatD is a cytoplasmic protein with DNase activity. No requirement for TatD family proteins in Sec-independent protein export, *J. Biol. Chem. 275*, 16717−16722.
21. Bilous, P. T., and Weiner, J. H. (1985) Dimethyl sulfoxide reductase activity by anaerobically grown *Escherichia coli* HB101, *J. Bacteriol. 162*, 1151−1155.
22. Sambasivarao, D., Dawson, H. A., Zhang, G., Shaw, G., Hu, J., and Weiner, J. H. (2001) Investigation of *Escherichia coli* dimethyl sulfoxide reductase assembly and processing in strains defective for the Sec-independent protein translocation system membrane targeting and translocation, *J. Biol. Chem. 276*, 20167−20174.
23. Markwell, M. A., Haas, S. M., Bieber, L. L., and Tolbert, N. E. (1978) A modification of the Lowry procedure to simplify protein determination in membrane and lipoprotein samples, *Anal. Biochem. 87*, 206−210.
24. Schagger, H., and von Jagow, G. (1987) Tricine-sodium dodecyl sulfate-polyacrylamide gel electrophoresis for the separation of proteins in the range from 1 to 100 kDa, *Anal. Biochem. 166*, 368−379.
25. Amin, D. N., Taylor, B. L., and Johnson, M. S. (2006) Topology and Boundaries of the Aerotaxis Receptor Aer in the Membrane of *Escherichia coli*, *J. Bacteriol. 188*, 894−901.
26. Lee, P. A., Buchanan, G., Stanley, N. R., Berks, B. C., and Palmer, T. (2002) Truncation analysis of TatA and TatB defines the minimal functional units required for protein translocation, *J. Bacteriol. 184*, 5871−5879.
27. van Gunsteren, W. F., Billeter, S. R., Eising, A. A., Hünenberger, P. H., Krüger, P., Mark, A. E., Scott, W. R. P., and Tironi, I. G. (1996) *Biomolecular Simulation: The GROMOS96 Manual and User Guide*, Vdf Hochschulverlag AG an der ETH Zürich, Zürich, Switzerland.
28. Guex, N., and Peitsch, M. C. (1997) SWISS-MODEL and the Swiss-PdbViewer: an environment for comparative protein modeling, *Electrophoresis 18*, 2714−2723.
29. Brunger, A. T., Adams, P. D., Clore, G. M., DeLano, W. L., Gros, P., Grosse-Kunstleve, R. W., Jiang, J. S., Kuszewski, J., Nilges, M., Pannu, N. S., Read, R. J., Rice, L. M., Simonson, T., and Warren, G. L. (1998) Crystallography & NMR system: A new software suite for macromolecular structure determination, *Acta. Crystallogr. D54*, 905−921.
30. Ash, W. L., Stockner, T., MacCallum, J. L., and Tieleman, D. P. (2004) Computer modeling of polyleucine-based coiled coil dimers in a realistic membrane environment: insight into helix-helix interactions in membrane proteins, *Biochemistry 43*, 9050−9060.
31. Engh, R. A., and Huber, R. (1991) Accurate bond and angle parameters for X-ray protein structure refinement, *Acta Crystallogr. A47*, 392−400.
32. DeLano, W. L. (2002) The PyMOL Molecular Graphics System, DeLano Scientific, San Carlos, CA.
33. Buchanan, G., de Leeuw, E., Stanley, N. R., Wexler, M., Berks, B. C., Sargent, F., and Palmer, T. (2002) Functional complexity of the twin-arginine translocase TatC component revealed by site-directed mutagenesis, *Mol. Microbiol. 43*, 1457−1470.

34. Barrett, C. M. L., Mathers, J. E., and Robinson, C. (2003) Identification of key regions within the *Escherichia coli* TatAB subunits, *FEBS Lett. 537*, 42−46.
35. Hicks, M. G., de Leeuw, E., Porcelli, I., Buchanan, G., Berks, B. C., and Palmer, T. (2003) The Escherichia coli twin-arginine translocase: conserved residues of TatA and TatB family components involved in protein transport, *FEBS Lett. 539*, 61−67.
36. Bogdanov, M., Zhang, W., Xie, J., and Dowhan, W. (2005) Transmembrane protein topology mapping by the substituted cysteine accessibility method (SCAM(TM)): application to lipid-specific membrane protein topogenesis, *Methods 36*, 148−171.
37. Seal, R. P., Leighton, B. H., and Amara, S. G. (2000) A model for the topology of excitatory amino acid transporters determined by the extracellular accessibility of substituted cysteines, *Neuron 25*, 695−706.
38. Mimura, H., Nakanishi, Y., Hirono, M., and Maeshima, M. (2004) Membrane topology of the H+-pyrophosphatase of *Streptomyces coelicolor* determined by cysteine-scanning mutagenesis, *J. Biol. Chem. 279*, 35106−35112.
39. Hu, Y. K., and Kaplan, J. H. (2000) Site-directed chemical labeling of extracellular loops in a membrane protein. The topology of the Na,K-ATPase alpha-subunit, *J. Biol. Chem. 275*, 19185−19191.
40. Boldog, T., and Hazelbauer, G. L. (2004) Accessibility of introduced cysteines in chemoreceptor transmembrane helices reveals boundaries interior to bracketing charged residues, *Protein Sci. 13*, 1466−1475.
41. Bogdanov, M., Heacock, P. N., and Dowhan, W. (2002) A polytopic membrane protein displays a reversible topology dependent on membrane lipid composition, *EMBO J. 21*, 2107−2116.
42. Loo, T. W., and Clarke, D. M. (1995) Membrane topology of a cysteine-less mutant of human P-glycoprotein, *J. Biol. Chem. 270*, 843−848.
43. Jung, H., Rubenhagen, R., Tebbe, S., Leifker, K., Tholema, N., Quick, M., and Schmid, R. (1998) Topology of the Na+/proline transporter of *Escherichia coli*, *J. Biol. Chem. 273*, 26400−26407.
44. Ye, L., Jia, Z., Jung, T., and Maloney, P. C. (2001) Topology of OxlT, the oxalate transporter of *Oxalobacter formigenes*, determined by site-directed fluorescence labeling, *J. Bacteriol. 183*, 2490−2496.
45. Grunewald, M., Menaker, D., and Kanner, B. I. (2002) Cysteine-scanning mutagenesis reveals a conformationally sensitive reentrant pore-loop in the glutamate transporter GLT-1, *J. Biol. Chem. 277*, 26074−26080.
46. Zhu, Q., Lee, D. W., and Casey, J. R. (2003) Novel topology in C-terminal region of the human plasma membrane anion exchanger, AE1, *J. Biol. Chem. 278*, 3112−3120.
47. Cao, W., and Matherly, L. H. (2004) Analysis of the membrane topology for transmembrane domains 7−12 of the human reduced folate carrier by scanning cysteine accessibility methods, *Biochem. J. 378*, 201−206.
48. Nagamori, S., Nishiyama, K., and Tokuda, H. (2002) Membrane topology inversion of SecG detected by labeling with a membrane-impermeable sulfhydryl reagent that causes a close association of SecG with SecA, *J. Biochem. (Tokyo) 132*, 629−634.
49. Long, J. C., Wang, S., and Vik, S. B. (1998) Membrane topology of subunit a of the F_1F_0 ATP synthase as determined by labeling of unique cysteine residues, *J. Biol. Chem. 273*, 16235−16240.
50. Wang, X., Bogdanov, M., and Dowhan, W. (2002) Topology of polytopic membrane protein subdomains is dictated by membrane phospholipid composition, *EMBO J. 21*, 5673−5681.
51. Sato, Y., Zhang, Y. W., Androutsellis-Theotokis, A., and Rudnick, G. (2004) Analysis of transmembrane domain 2 of rat serotonin transporter by cysteine scanning mutagenesis, *J. Biol. Chem. 279*, 22926−22933.
52. Hughson, A. G., and Hazelbauer, G. L. (1996) Detecting the conformational change of transmembrane signaling in a bacterial chemoreceptor by measuring effects on disulfide cross-linking *in vivo*, *Proc. Natl. Acad. Sci. U.S.A. 93*, 11546−11551.
53. Lee, G. F., Burrows, G. G., Lebert, M. R., Dutton, D. P., and Hazelbauer, G. L. (1994) Deducing the organization of a transmembrane domain by disulfide cross- linking. The bacterial chemoreceptor Trg, *J. Biol. Chem. 269*, 29920−29927.
54. Lee, P. A., Tullman-Ercek, D., and Georgiou, G. (2006) The Bacterial Twin-Arginine Translocation Pathway, *Annu. Rev. Microbiol. 60*, 373−395.
55. Hoffmann, K., and Stoffel, W. (1993) TMbase - A database of membrane spanning protein segments, *Biol. Chem. Hoppe-Seyler 374*, 166.
56. Heijne, G. V. (1986) The distribution of positively charged residues in bacterial inner membrane proteins correlates with the transmembrane topology, *EMBO J. 5*, 3021−3027.
57. Bowie, J. U. (2006) Flip-flopping membrane proteins, *Nat. Struct. Mol. Biol. 13*, 94−96.

BI7005288